DRAFT VERSION APRIL 21, 2015
Preprint typeset using LaTeX style emulateapj v. 05/12/14

A DYNAMICAL STUDY OF THE BLACK HOLE X-RAY BINARY NOVA MUSCAE 1991[1]

Jianfeng Wu[2], Jerome A. Orosz[3], Jeffrey E. McClintock[2], Danny Steeghs[4,2], Penélope Longa-Peña[4], Paul J. Callanan[5], Lijun Gou[6], Luis C. Ho[7,8], Peter G. Jonker[9,10,2], Mark T. Reynolds[11], Manuel A. P. Torres[9,10]

ApJ in press

ABSTRACT

We present a dynamical study of the Galactic black hole binary system Nova Muscae 1991 (GS/GRS 1124−683). We utilize 72 high resolution Magellan Echellette (MagE) spectra and 72 strictly simultaneous V-band photometric observations; the simultaneity is a unique and crucial feature of this dynamical study. The data were taken on two consecutive nights and cover the full 10.4-hour orbital cycle. The radial velocities of the secondary star are determined by cross-correlating the object spectra with the best-match template spectrum obtained using the same instrument configuration. Based on our independent analysis of five orders of the echellette spectrum, the semi-amplitude of the radial velocity of the secondary is measured to be $K_2 = 406.8 \pm 2.7$ km s^{-1}, which is consistent with previous work, while the uncertainty is reduced by a factor of 3. The corresponding mass function is $f(M) = 3.02 \pm 0.06\,M_\odot$. We have also obtained an accurate measurement of the rotational broadening of the stellar absorption lines ($v \sin i = 85.0 \pm 2.6$ km s^{-1}) and hence the mass ratio of the system $q = 0.079 \pm 0.007$. Finally, we have measured the spectrum of the non-stellar component of emission that veils the spectrum of the secondary. In a future paper, we will use our veiling-corrected spectrum of the secondary and accurate values of K_2 and q to model multi-color light curves and determine the systemic inclination and the mass of the black hole.

Subject headings: black hole physics — stars: black holes — binaries: general — X-rays: binaries

1. INTRODUCTION

Mass is the fundamental parameter for a black hole. According to the No-Hair Theorem (e.g., Israel 1967; Hawking 1971), mass and spin together provide a complete description of an astrophysical black hole. An accurate measurement of mass is a prerequisite for measuring black hole spin via the continuum-fitting method (see McClintock et al. 2014 for a review). Stellar-mass black holes in the Milky Way and neighboring galaxies are discovered in X-ray binary systems, some of which are persistent X-ray sources, while others are X-ray transients which have gone through one or more X-ray outbursts (Remillard & McClintock 2006). About two dozen of these black holes have been dynamically confirmed to have masses in the range $M = 5$–$30\,M_\odot$.

X-ray Nova Muscae 1991 (hereafter NovaMus), with an orbital period of 10.4 hr, is one of about a dozen black-hole transient systems that are distinguished by their short orbital periods, $P < 12$ hr. (For a sketch to scale of nine of these systems, including the prototype A0620−00, see Figure 1 in McClintock et al. 2014.) NovaMus was discovered during its 1991 outburst independently by the *Ginga* (Makino et al. 1991) and *GRANAT* (Lund & Brandt 1991) missions. Eight days after discovery, it reached a peak X-ray intensity of 8 Crab in the 1–6 keV band (Ebisawa et al. 1994). Over the course of eight months, the source passed through all the canonical X-ray states before returning to its quiescent state (Ebisawa et al. 1994; Remillard & McClintock 2006). Esin et al. (1997) used the 1991 outburst data for NovaMus to develop a model of the states that combines the standard model of a thin accretion disk (Shakura & Sunyaev 1973) and the advection-dominated accretion flow (ADAF) model (Narayan & Yi 1994).

Interestingly, hard X-ray observations of NovaMus made at the peak of the outburst revealed evidence for positron-electron annihilation in the form of a relatively narrow and variable emission line near 500 keV (Sunyaev et al. 1992; Goldwurm et al. 1992). Kaiser & Hannikainen (2002) argued that the line could be generated by annihilation in the bipolar outflow of the system. Martín et al. (1996) suggested an alternative mechanism, namely, Li production near the black hole that gives rise to a 476 keV nuclear line; their supporting evidence is their detection of a relatively strong lithium absorption line $\lambda 6708$ in the optical spectrum.

Soon after its discovery, NovaMus was considered to be a strong candidate for a black hole binary based on its X-ray spectral properties and light curve, and its similarities to the prototype black-hole X-ray transient A0620−00 (McClintock & Remillard 1986). Following the discovery of the optical counterpart (Della Valle et al. 1991), the black hole nature of the primary was established in the customary way by measuring the mass function:

$$f(M) \equiv \frac{PK_2^3}{2\pi G} = \frac{M \sin^3 i}{(1+q)^2}, \quad (1)$$

jianfeng.wu@cfa.harvard.edu

[1] This paper includes data gathered with the 6.5 meter Magellan Telescopes located at Las Campanas Observatory, Chile.

[2] Harvard-Smithsonian Center for Astrophysics, 60 Garden Street, Cambridge, MA 02138, USA
[3] Department of Astronomy, San Diego State University, 5500 Campanile Drive, San Diego, CA 92182, USA
[4] Department of Physics, University of Warwick, Coventry, CV4 7AL, UK
[5] Department of Physics, University College Cork, Cork, Ireland
[6] National Astronomical Observatories, Chinese Academy of Sciences, Beijing 100012, China
[7] Kavli Institute for Astronomy and Astrophysics, Peking University, Beijing 100871, China
[8] Department of Astronomy, School of Physics, Peking University, Beijing 100871, China
[9] SRON, Netherlands Institute for Space Research, Sorbonnelaan 2, 3584 CA, Utrecht, The Netherlands
[10] Department of Astrophysics/IMAPP, Radboud University Nijmegen, Heyendaalseweg 135, 6525 AJ, Nijmegen, The Netherlands
[11] Department of Astronomy, University of Michigan, 1085 S. University Avenue, Ann Arbor, MI 48109, USA

where K_2 is the semi-amplitude of the velocity curve of the secondary, i is the orbital inclination angle of the binary and q is the ratio of the companion star mass M_2 to that of the compact primary M. Three dynamical studies performed in quiescence found a value for the mass function (the minimum mass of the compact primary) of $\approx 3M_\odot$ (Remillard et al. 1992; Orosz et al. 1996; Casares et al. 1997), which is widely considered to be the maximum stable mass of a neutron star (Kalogera & Baym 1996).

Orosz et al. (1994) obtained a quite uncertain estimate of the mass ratio $q \equiv M_2/M$ by measuring the radial velocity of the Hα emission line. Casares et al. (1997) made a conventional and direct measurement of the mass ratio by measuring the rotational broadening of the photospheric absorption lines of the secondary; they obtained a result that is consistent with that of Orosz et al. (1994).

The inclination angle i is usually estimated by modeling the ellipsoidal modulation of the light curves of the secondary star after a system has returned to its quiescent state. This modeling is complicated in the case of the short-period systems because the stellar component of light is significantly contaminated by the emission from the accretion disk; this so-called "disk veiling," can be quite significant ($\gtrsim 50\%$ in the V-band) and variable in "active" quiescent states (Cantrell et al. 2010). Orosz et al. (1996) estimated a disk contribution at ~ 5000 Å that could be as high as 50%. Meantime, using different data, Casares et al. (1997) estimated a disk contribution at Hα λ6563 of 15%, suggesting that disk veiling may be less significant at longer wavelengths. Based on this notion, Gelino et al. (2001) modeled near-infrared (J and K) light curves of NovaMus assuming that the disk contribution could be ignored in these bands, and they thereby estimated the systemic inclination to be $i = 54^\circ \pm 1.5^\circ$; their estimate of black hole mass (which also depends on the mass ratio q) is $M = 6.95 \pm 0.6\,M_\odot$.

These estimates of i and M are quite uncertain because they rest on the assumption that the effects of veiling are negligible in the near-infrared, while there is considerable evidence that it may not be (e.g., Reynolds et al. 2007, 2008; Kreidberg et al. 2012). In this paper, we obtain the first detailed and secure measurement of the spectrum of the non-stellar component of light that veils the stellar spectrum. While this achievement is in part due to the quality and quantity of our data, it is based primarily on the strict simultaneity of our spectroscopic and photometric observations. The simultaneity is crucial because of the aperiodic variability of the non-stellar component. Our two other principal results are a greatly refined measurement of the K-velocity and the first robust measurement of the mass ratio q, which differs significantly from the earlier estimates mentioned above.

This paper is structured as follows. Observations and data reduction are described in §2. We derive the mass function via a radial velocity analysis in §3. The mass ratio is determined via rotational broadening in §4. The disk veiling is also measured in this section. The light curve of NovaMus is presented in §5. Finally, we discuss our results in §6. The light curve modeling and the determination of the inclination and black hole mass will be presented in a subsequent paper.

2. OBSERVATION AND DATA REDUCTION

2.1. *Magellan Echellette Spectroscopy*

The spectroscopic data were obtained using the Magellan Echellette spectrograph (MagE; Marshall et al. 2008) mounted on the 6.5-meter Magellan/Clay Telescope at the Las Campanas Observatory (LCO) in Chile. All the data were taken on the nights of 2009 April 25–26 UT. A total of 72 spectra were obtained, each with an integration time of 600 s. During the same two nights, and with the same setup, we obtained spectra of 38 stars, principally K dwarfs, that serve as radial velocity templates. The seeing was similar on both nights, with a typical value of $\approx 0.7''$ and a range of $0.5''$–$1.3''$. Each MagE spectrum consists of 15 orders (corresponding to sequence numbers #6–20). The full wavelength coverage of the instrument is 3100–11000 Å, with order #20 at the blue end (central wavelength 3125 Å) and order #6 at the red end (central wavelength 9700 Å). The spatial scale is $\approx 0.3''$/pixel. The spectral dispersion increases from 0.2 Å per pixel for order #20 to 0.7 Å per pixel for order #6, while the velocity dispersion is 22 km s^{-1} per pixel for all orders. For our chosen $0.85''$ slit, the spectral resolution is ≈ 1 Å at 5000 Å, corresponding to ≈ 60 km s^{-1}.

The MagE data were reduced using the pipeline developed by Carnegie Observatories[12], which performs bias correction, flat-fielding, and wavelength calibration. The bias was corrected using the overscan region of the detectors. Three sets of flats were utilized in the calibration: 1) order definition flats taken with the Xe-Flash lamps; 2) blue flats to define the flat field at the blue end of a spectrum (also taken with the Xe-Flash lamps); and 3) red flats to define the flat field at the red end of a spectrum and to correct the fringing, which were taken with the Qf lamps. The wavelength calibration was performed using arc spectra obtained with Thorium-Argon lamps. The RMS residual of the wavelength solution is < 0.05 Å for orders #8–18 and < 0.1 Å for the remaining orders. The performance of wavelength calibration was examined using sky emission lines; the relative wavelength offset is negligible.

The mean MagE spectrum of NovaMus in the observer's rest-frame is shown in Fig. 1, which covers spectra that span orders #9–14 ($\sim$ 4300–7000 Å). The spectrum in each order was normalized by a fifth-order polynomial. In the analysis that follows, we mainly use the data in these orders because of their good signal-to-noise (S/N) ratio and general lack of sky emission lines and telluric absorption features (relative to redder orders). The most prominent features in the spectrum are the broad, double-peaked Balmer lines Hα λ6563, Hβ λ4861 and Hγ λ4341, which are the canonical signatures of a black-hole accretion disk. Also present are broad disk lines of He, notably He I λ5875. Other features such as Na D $\lambda\lambda$5890–5896, diffuse interstellar bands (DIB) at λ5780, λ6280, and telluric features redward of λ6850 are also evident.

2.2. *Optical Photometry*

Photometric data were obtained during the same observing run using the du Pont 2.5 m telescope, which is also located at LCO. Seventy-two V-band images were acquired; by design, each 10-min exposure was strictly simultaneous (time difference < 1 s) with its corresponding MagE spectroscopic observation[13]. The typical seeing was $\approx 0.7''$ (with a range of 0.6–$1.1''$). We used the 2048×2048 Tek#5 CCD, which provided a field of view of $8.85' \times 8.85'$ at $0.259''$ per pixel. Bias correction and flat-fielding were performed with standard IRAF

[12] See http://code.obs.carnegiescience.edu/mage-pipeline.

[13] The only exception is the first image whose exposure time was only 60 seconds.

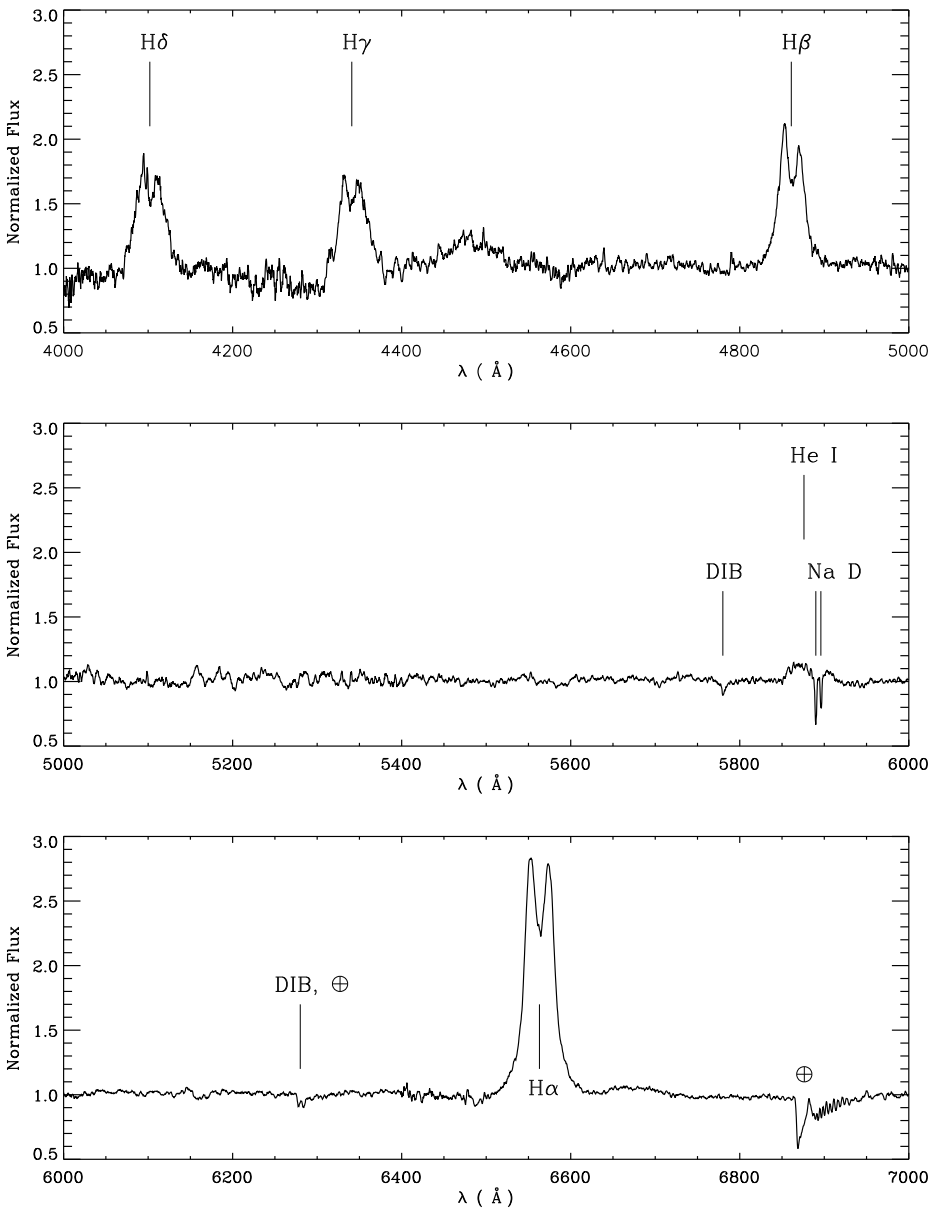

FIG. 1.— The mean Magellan/MagE spectrum of NovaMus in the observer's rest frame, covering MagE orders #9–14 (4000–7000 Å). Broad and double-peaked Balmer lines (Hα, Hβ, Hγ, and Hδ) are prominent in the spectrum. He I λ5875 emission is also evident. The weak, broad emission features redward of Hγ and Hα are likely to be He I λ4471 and λ6678, respectively. The Na D $\lambda\lambda$5890–5896 doublet, DIB features at λ5780 and λ6280 (which also has a strong telluric component), as well as the telluric feature at λ6860 are also labeled. The NovaMus spectrum covering the full MagE wavelength range ($\sim$ 3000–10000 Å) is available in the online journal in electronic form.

tasks (`zerocombine`, `flatcombine`, and `ccdproc`). The centroid of the optical counterpart was determined using the CIAO routine `wavdetect` (Freeman et al. 2002), and the quality of the centroiding was confirmed visually. Aperture photometry was performed using the IDL procedure `aper`. The radius of the aperture was fixed to eight pixels (2.1″), which is the largest aperture that securely excludes significant contamination of NovaMus by a faint field star. Choosing a smaller aperture (e.g., $\sim$ 5 pixels) would provide very similar results. We first produced a light curve of NovaMus relative to nearby field stars and then derived an absolute calibration relative to a pair of nearby (24″ and 41″) standard stars. Our estimate of the uncertainty in the zero-point is 0.05 mag.

3. RADIAL VELOCITY ANALYSIS

The radial velocity K_2 of the secondary star was determined by sequentially cross-correlating the 72 object spectra with the spectrum of a template star. This was done in turn for individual echellette orders, rather than using a single merged spectrum. The best quality results were obtained for order #12 (covering $\sim$ 4700–5500 Å), as expected since strong stellar absorption features are present in this order (e.g., the Mg

TABLE 1
RADIAL VELOCITY ANALYSIS RESULTS

Order #	K_2 (km s^{-1})	γ (km s^{-1})	$T_0 - 2454900$ (d)	No. of Object Spectra	χ^2/ν	λ Coverage (Å)	Masked Features
9[a]	413.6 ± 4.3	17.4 ± 3.1	46.90550 ± 0.00072	39	1.55	6300–7300	Hα λ6563, 6820–7020 Å, 7150–7200 Å
10	409.5 ± 2.7	19.4 ± 2.0	46.90351 ± 0.00044	72	0.92	5680–6630	Na D $\lambda\lambda$5890, 5896, DIB λ6280 O I λ6300, Hα λ6563
11	413.0 ± 3.1	15.2 ± 2.3	46.90258 ± 0.00051	67	0.74	5170–6000	O I λ5577, Na D $\lambda\lambda$5890, 5896
12	401.2 ± 2.6	9.7 ± 1.9	46.90327 ± 0.00044	72	0.87	4700–5500	Hβ λ4861
13	407.0 ± 4.2	17.0 ± 3.1	46.90211 ± 0.00069	57	0.92	4370–5100	Hβ λ4861
14	403.9 ± 3.9	9.2 ± 2.9	46.90086 ± 0.00068	63	1.02	4060–4730	Hγ λ4341
Average	406.8 ± 2.2	14.2 ± 2.1	46.90278 ± 0.00042				

NOTE. — The quoted uncertainties are at the 1σ level of confidence.

[a] The best-fit parameters for order #9 were not included in calculating the average parameter values; for this order, the wavelength ranges 6820–7020 Å and 7150–7200 Å were masked to avoid strong telluric absorption features and sky emission lines.

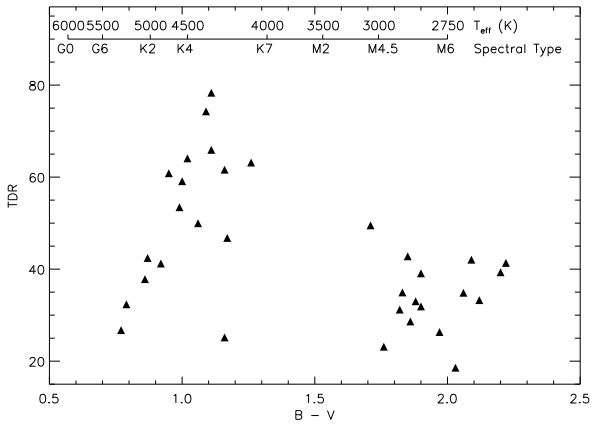

FIG. 2.— The average TDR value of the cross-correlation between the spectrum of each template star and NovaMus for order #12, plotted against the $B-V$ color of the star. The template star with the highest average TDR value is HD 170493, with $B-V = 1.11$, which corresponds to a spectral type of $\sim$K5 with $T_{\rm eff} \approx 4400$ K, based on the scale of $B-V$ color vs. $T_{\rm eff}$ vs. Spectral type, which is shown at the top of the figure.

features at $\sim$5200 Å region), and it is relatively free of contaminating telluric and interstellar features.

3.1. *Choosing the Best Template Spectrum*

The cross-correlation analysis was performed using the software package `fxcor` as implemented in the IRAF package. The task `fxcor` returns the parameter R defined by Tonry & Davis (1979; TDR hereafter) provides an estimate of S/N: the higher the TDR value, the better the quality of the cross-correlation. From among our dozens of template spectra, we chose the one that gives the highest TDR value, while focusing on the NovaMus data for order #12. Specifically, we: (1) selected a K-type template spectrum that gives relatively high values of TDR and cross-correlated it against the 72 spectra of NovaMus; (2) we velocity-shifted all the NovaMus spectra to the rest frame of the template star and summed them; (3) we then cross-correlated this summed spectrum against all of our template spectra in turn and selected the template spectrum that yielded the maximum TDR value.

The results of this analysis are summarized in Fig. 2, which shows how TDR varies among the template stars, which we have ordered by their $B-V$ color given in the SIMBAD database; we regard the photometric color as a more accurate measure of the effective temperature than the spectral type (that is given in the same database)[14]. The star at the peak of this ordered distribution and having the maximum TDR is HD 170493 with $B-V = 1.11$, corresponds to an effective temperature $T_{\rm eff} \approx 4400$ K (*Allen's Astrophysical Quantities, 4th edn.*). We therefore choose HD 170493 as the master template for our cross-correlation analysis. Potential systematic effects related to this choice of template are discussed in §6.1.

3.2. *Fitting the Radial Velocity Curve*

With HD 170493 as the template, we first cross-correlated each of the 72 spectra for order #12. For both the object and template spectra, we masked out the region around the Hβ emission line, and also $\sim$ 100 Å at both ends of each order because the S/N in these regions is poor. We furthermore required that the TDR value for a correlation exceed 2.5 (similar to the criterion in Orosz et al. 1996). All 72 spectra for order #12 delivered reliable measurements of radial velocity, as illustrated in the middle-right panel of Fig. 3. We fitted the radial velocity curve with the following model,

$$V(t) = \gamma + K_2 \cos(2\pi \frac{t - T_0}{P}), \qquad (2)$$

where γ is the systemic velocity of in the heliocentric frame, t is the observation time in Heliocentric Julian Days (HJDs), and T_0 is the time of maximum radial velocity; the radial velocity we used for the template star HD 170493 is $\gamma_0 = -55.07 \pm 0.07$ km s^{-1}. We initially fixed the orbital period to the spectroscopic value given by Orosz et al. (1996), $P = 0.4326058(31)$ d. Then, using our value of T_0 and the one in Orosz et al. we obtained a refined value of the orbital period: $P = 0.43260249(9)$ d. This period and other best-fit parameters are listed in Table 1.

As a check on our value for the K-velocity, we performed an independent analysis using the `xcor` procedure in the MOLLY package developed by T. Marsh[15] in place of `fxcor` in IRAF. We again analyzed only the data for order #12 and used the same template spectrum (HD 170493) as before. Both the object and template spectra were rebinned to the same velocity dispersion using the `vbin` procedure, and were normalized using a fifth-order polynomial, as required by the `xcor` procedure. Fitting a Gaussian to the profile of the cross-correlation function using the MOLLY procedure `mgfit`, we

[14] We assume that the reddening of these template star can be ignored due to their proximity to the Sun ($\lesssim$ 100 pc).

[15] See http://deneb.astro.warwick.ac.uk/phsaap/software/molly/html/INDEX.html.

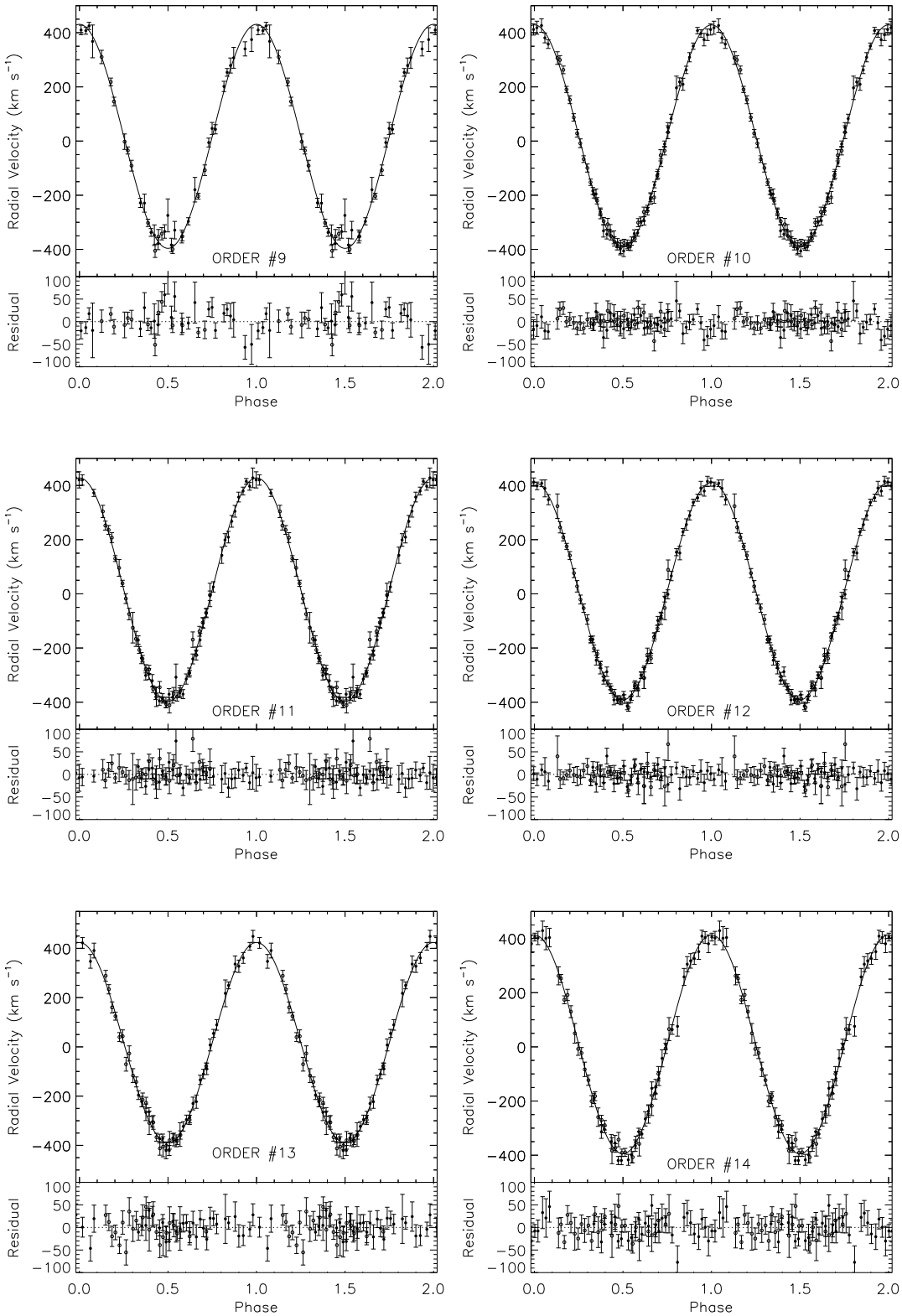

FIG. 3.— The radial velocities of NovaMus relative to the spectral template HD 170493, in MagE orders #9–14. The best-fit radial velocity curves and residuals for each order are shown.

TABLE 2
ORBITAL PARAMETERS FOR NOVAMUS

Parameter	Value
Orbital period P (days)	$0.43260249 \pm 0.00000009$
K_2 velocity (km s^{-1})	406.8 ± 2.7
γ velocity (km s^{-1})	14.2 ± 6.3
T_0, spectroscopic (HJD$-$2454900)	46.90278 ± 0.00062
Mass function $f(M)$ ($M_\odot$)	3.02 ± 0.06
$v \sin i$ (km s^{-1})	85.0 ± 2.6
Mass ratio q	0.079 ± 0.007

NOTE. — The quoted uncertainties are at the 1σ level of confidence and include an allowance for systematic error; see §6.1.

obtained values for both the K-velocity and its uncertainty ($K_2 = 402.9 \pm 1.3$ km s^{-1}) that are consistent with those obtained using the IRAF routines.

In order to obtain a more precise value of K_2, we analyzed data for orders #10 and #11 (which lie to the red of order #12) and orders #13 and #14, again masking out ~ 100 Å at both ends of each order; the wavelength ranges of the orders are given in Table 1. As before, we masked out disk emission lines (mainly Balmer lines), and we also masked out a number of strong telluric and interstellar features, which are listed in Table 1). As was the case for order #12 discussed above, all 72 object spectra for order #10 yielded reliable measurements of radial velocity (i.e., TDR > 2.5); the radial velocity curve for this order is shown in Fig. 3. For the other three orders, some object spectra were rejected because: (1) the TDR value for the correlation was ≤ 2.5; (2) the fit to the cross-correlation peak did not converge; or (3) the value obtained for the radial velocity lies more than $\gtrsim 3\sigma$ away from the fitted curve.[16] The velocity data for each order individually were fitted to the same model used for order #12 (Eqn. 2). For each of the five orders, Table 1 lists the best-fit parameters, values of reduced χ^2 and the number of useful spectra. Using precisely the velocity uncertainties returned by `fxcor`, we obtain good fits for all five orders, with χ^2/ν values that are close to unity. We note that there are small differences among the best-fit parameters at the level of ~ 3–4σ level.

Table 2 provides a summary of the orbital parameters. The error-weighted mean of K_2 among the five orders is 406.8 ± 2.2 km s^{-1}. After including our estimate of the systematic error (see §6.1), we obtain for the radial velocity semi-amplitude $K_2 = 406.8 \pm 2.7$ km s^{-1}. Using this value of K_2, the orbital period P (Table 2) and Eqn. (1), we derive a precise value for the mass function of $f(M) = 3.02 \pm 0.06\ M_\odot$, thereby confirming the black hole nature of the compact object.

In addition to orders #10–14, and as discussed in the following section, we also performed a radial velocity analysis of order #9 for the purpose of measuring the mass ratio q and investigating the effects of disk veiling. The best-fit parameters for order #9 are included in Table 1. However, we do not include the results for this order in our final determination of the radial velocity parameters because relatively few spectra generated useful velocity data (39 out of 72) and because the quality of the fit is relatively poor ($\chi^2/\nu = 1.55$).

[16] Only five data points in all five orders lie $\gtrsim 3$–4σ away from the fitted curve; removing these radial velocity points does not significantly change the fitted values of the parameters.

4. ROTATIONAL VELOCITY AND DISK VEILING MEASUREMENTS

4.1. *Rotational Broadening and Mass Ratio*

As the next step toward measuring the mass of the black hole, we obtain a precise estimate of the mass ratio q. For a short-period, mass-exchange binary like NovaMus, one can quite confidently assume that the system is tidally-locked and that the secondary fills its Roche lobe (Wade & Horne 1998). In this case, q can be simply determined by measuring the rotational broadening of the stellar photospheric lines. Specifically, one measures the radial component of the rotational velocity of the secondary star, $v \sin i$ and uses the following equation (Wade & Horne 1998),

$$\frac{v \sin i}{K_2} = 0.462 q^{1/3} (1+q)^{2/3}. \quad (3)$$

In measuring $v \sin i$ we use the method of *optimal subtraction*. Fig. 4 illustrates the principle of the method using the data for orders #10 and #12. Before doing the optimal subtraction, we first normalized both the object and template spectra using a 5th-order polynomial. The spectra of NovaMus contains contributions from both the secondary (numerous rotationally-broadened absorption features) and the accretion disk (broad disk emission lines like Hα). The best-match template spectrum will have virtually the same set of absorption features as NovaMus; however, the features in the object spectrum will be shallower because they are diluted by the disk continuum emission. In obtaining the best match of a given template spectrum to the object spectrum, one repetitively performs a pair of operations. First, one broadens the narrow-line template spectrum, and then multiplies the spectrum by the factor $f_{\rm star}$ ($0 \leqslant f_{\rm star} \leqslant 1$), which represents the fraction of the light contributed by the secondary. Finally, one subtracts the trial template spectrum from the spectrum of NovaMus and determines quantitatively (see below) the template spectrum that is freest of photospheric absorption features. The results of such an analysis for two orders are shown in Fig. 4. The residual spectrum for order #10 (upper panel) only shows the broad Hα disk line and the DIB at $\lambda 6280$. The only clear spectral feature in the residual spectrum of order #12 (Fig. 4; lower panel) is the Fe II multiplet 42 at $\lambda 4924$, $\lambda 5018$, and $\lambda 5169$ (Moore 1972), a feature that is also present in the spectra of A0620$-$00 (Marsh et al. 1994) and the neutron-star transient EXO 0748$-$676 (Ratti et al. 2012).

In practice, we use the spectrum of our velocity-template star HD 170493 and the phase-averaged spectra of NovaMus for each order to increase the S/N. Before averaging the spectra for a given order, we shifted the individual spectra to the rest frame of HD 170493 using the data in Table 1. We first broadened the template spectrum using a grid of trial values from 5 to 300 km s^{-1} in steps of 5 km s^{-1}. We also artificially smeared the template spectrum using the appropriate phase and integration time in order to simulate the velocity smearing during an observation of NovaMus. A χ^2 test was performed on the residual spectrum to determine a minimum and the corresponding approximate value of $v \sin i$. Now, starting with this approximate value, we repeated the procedure with a trial grid extending from 60 to 120 km s^{-1} in steps of 1 km s^{-1}. Making use of the `rbroad` and `optsub` tasks in the MOLLY, curves of $v \sin i$ vs. χ^2 were generated (see Fig. 5) and fitted with a 3rd-order polynomial; our adopted value of $v \sin i$ corresponds to the minimum of the fitted curve. All the

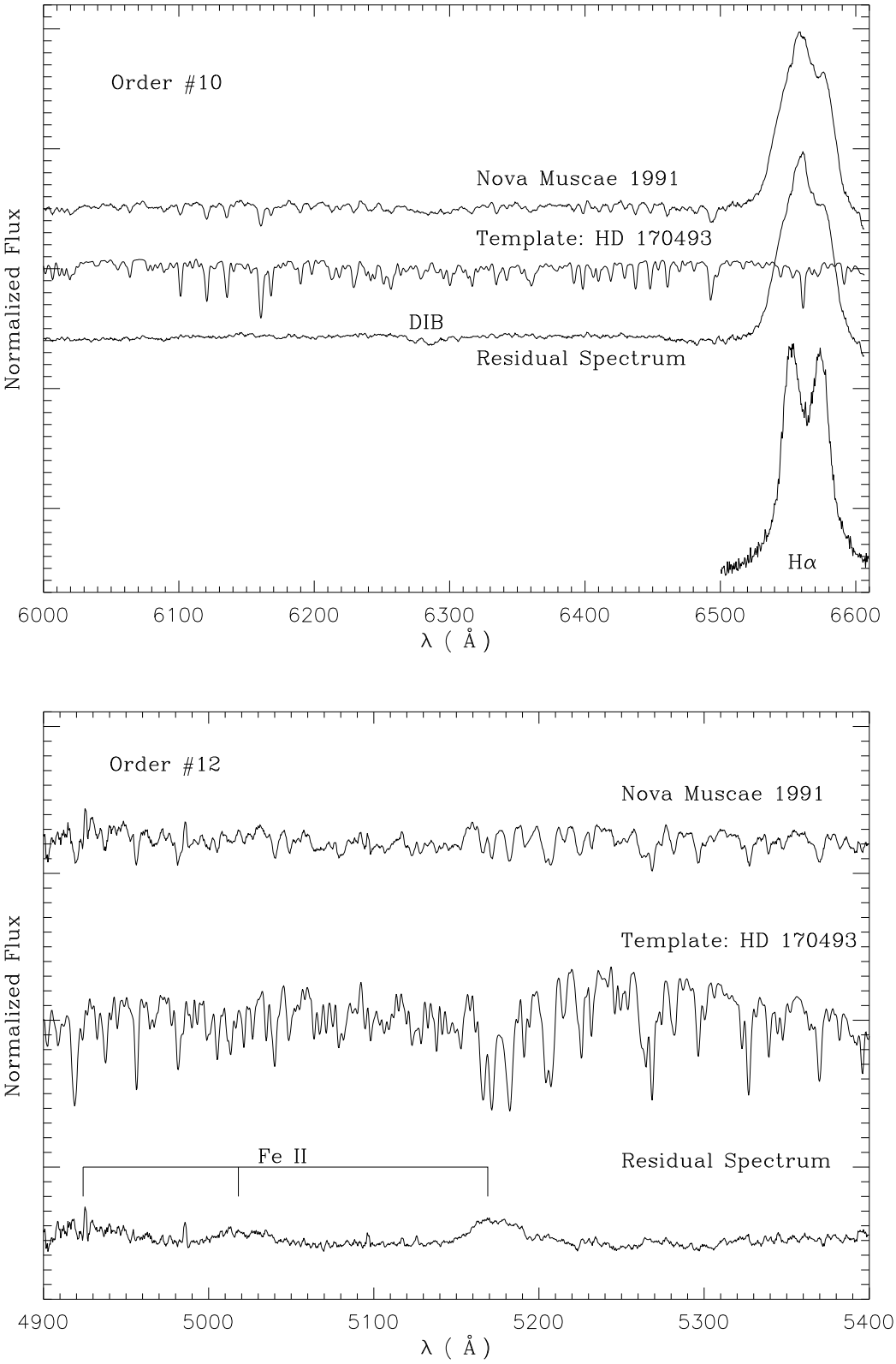

FIG. 4.— The results of applying the optimal subtraction procedure for order #10 (upper panel) and order #12 (lower panel). Each panel contains the average normalized spectrum of NovaMus, the normalized spectrum of the template star HD 170493, and the residual spectrum after optimal subtraction. The Hα emission line and strong DIB feature are labeled for order #10. The upper panel also contains the averaged Hα emission line in the observer's frame, which shows the characteristic double-peaked profile. The Fe II multiplet 42 features in the residual spectrum of order #12 are labeled in the lower panel. All the spectra are smoothed with a 5-pixel boxcar for the purpose of presentation.

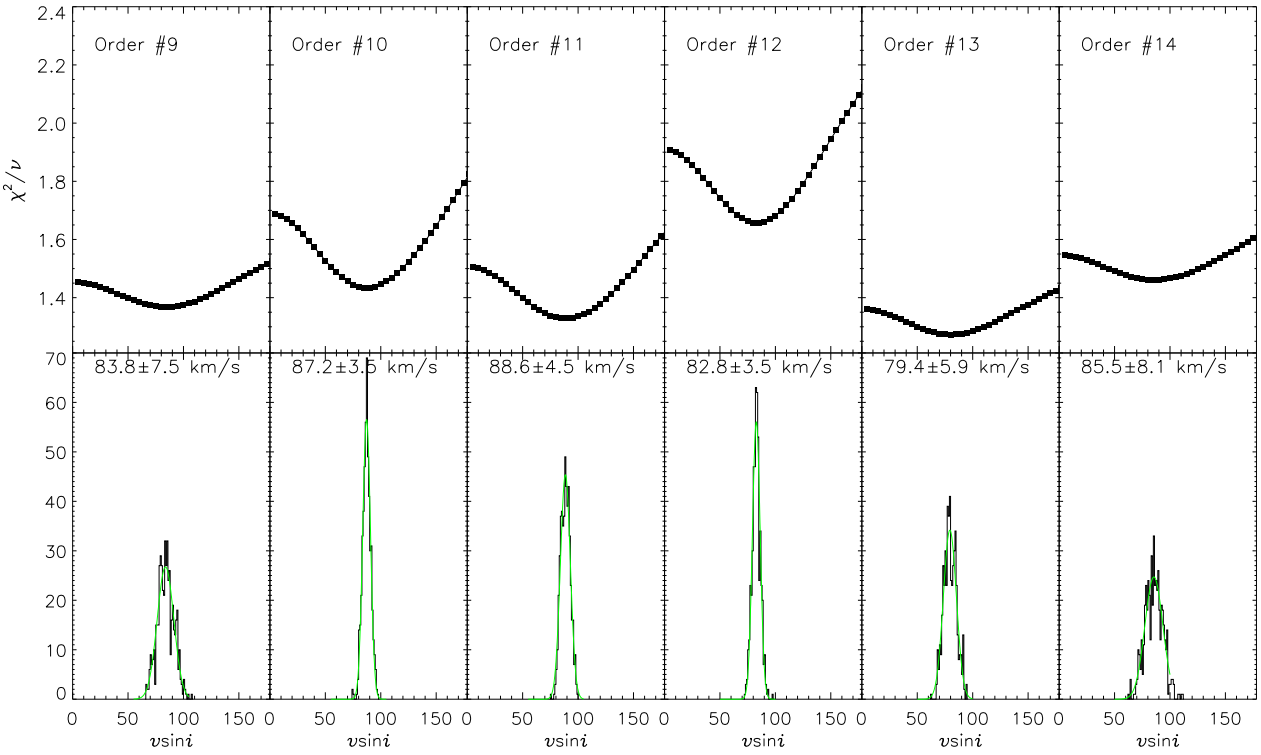

FIG. 5.— Measurement of the rotational velocity $v\sin i$ in MagE orders #9–14. For each order, the upper panel shows the curve of $v\sin i$ vs. χ^2, which we fitted with a cubic polynomial. Our adopted value of $v\sin i$ is the value corresponding to the minimum in χ^2. The lower panel illustrates the method we used to estimate the uncertainty in $v\sin i$ via the bootstrap method described in the text. The histogram of $v\sin i$ is fitted with a Gaussian in determining the uncertainty.

emission lines, interstellar features, and telluric features are masked out during the optimal subtraction.

The effect of limb darkening needs to be properly considered in the optimal subtraction. Since this effect varies with wavelength, we calculated a linear limb darkening coefficient for each order of the MagE spectra based on the data given by Claret et al. (2012). We retrieved from their table the limb darkening coefficients for the *UBVRI* bands. For the effective temperature of the companion star, we adopted the value $T_{\rm eff} = 4400$ K. The star's surface gravity $\log g$ (in cm^{-2} s^{-1}) is securely in the range 4.0–4.5, and for each band we adopted the average of the tabulated values of the limb darkening coefficient for $\log g = 4.0$ and $\log g = 4.5$. Finally we linearly interpolated between the *UBVRI* bands using the central wavelength of each order, thereby obtaining the values we adopt for the limb darkening coefficients (see the third column in Table 3), which range from 0.71 (Order #9) to 0.91 (Order #14).

We utilized the bootstrap method to determine the uncertainty in $v\sin i$ following Steeghs & Jonker (2007) and Ratti et al. (2013). We generated 500 simulated NovaMus spectra using the MOLLY task `boot`. The bootstrap method randomly selects data points from the original spectrum while keeping the same total number of data points in the spectrum. For each simulated spectrum, $v\sin i$ was measured following the same procedure as described above. The 500 $v\sin i$ values follow a Gaussian distribution (see Fig. 5). The mean of the Gaussian distribution is very close (within 1 km s^{-1}) to the fitted values of $v\sin i$ discussed above. For each order, we take the mean of the Gaussian distribution as the final measurement of $v\sin i$ and the standard deviation of the mean σ as the uncertainty. The measured values of $v\sin i$ for six orders (#9–14) are presented in Fig. 5 and Table 3).

TABLE 3
LIMB DARKENING COEFFICIENT AND ROTATIONAL VELOCITY

Order #	Central λ (Å)	u (limb darkening)	$v\sin i$ (km s^{-1})	Disk Veiling (%)
9	6800	0.706	83.8 ± 7.5	40.3 ± 3.4
10	6130	0.762	87.2 ± 3.5	51.4 ± 1.3
11	5590	0.808	88.6 ± 4.5	56.7 ± 1.4
12	5140	0.845	82.8 ± 3.5	59.3 ± 1.0
13	4750	0.878	79.4 ± 5.9	55.8 ± 2.1
14	4400	0.908	85.5 ± 7.1	69.1 ± 1.5
Average			85.0 ± 1.3	

NOTE. — The quoted uncertainties are at the 1σ level of confidence.

The error-weighted mean $v\sin i$ of all six orders is $\langle v\sin i \rangle = 85.0 \pm 1.3$ km s^{-1}. After including an allowance for systematic uncertainty, related to the choice of template spectrum and the limb darkening coefficient (see §6.1), our final adopted value is $v\sin i = 85.0 \pm 2.6$ km s^{-1}. Using this value and our K-velocity for the secondary ($K_2 = 406.8 \pm 2.7$ km s^{-1}; §3.2), and Eqn. (3), we obtain for the mass ratio the value $q = 0.079 \pm 0.007$. Using this mass ra-

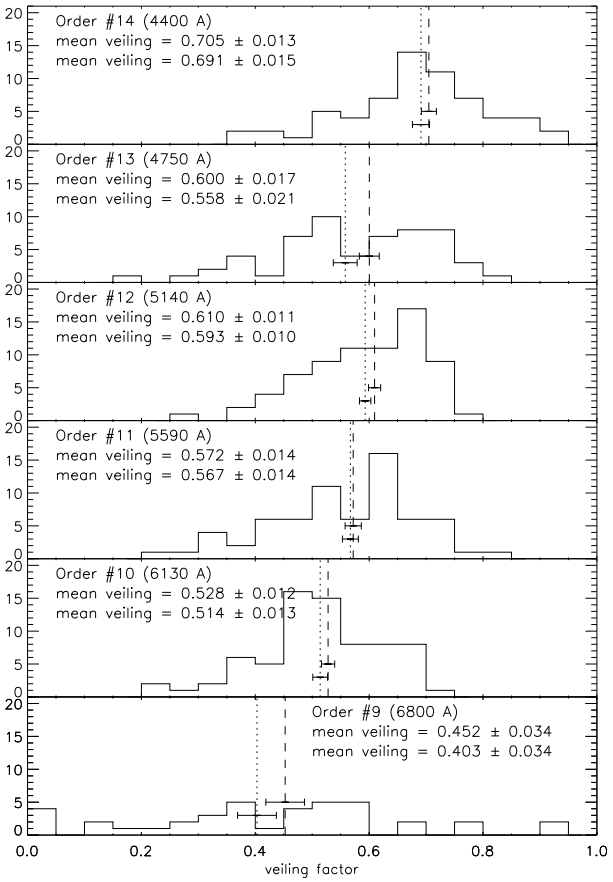

FIG. 6.— Measurement of the disk veiling fraction in order #9–14. In each panel, the dotted line indicates the disk veiling fraction (labeled by the "mean veiling 1" value) of the averaged spectrum. The histogram shows our disk veiling measurements for individual spectra; the dashed line indicates their mean value as obtained from the histogram (labeled by the "mean veiling 2" value).

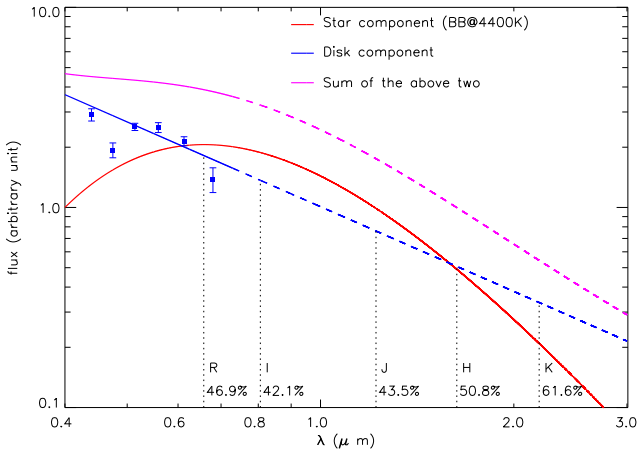

FIG. 7.— The simplistic spectral energy distribution of NovaMus, decomposed into the secondary star component (red line) and the accretion disk component (blue line). The pink line shows the sum of the two components. The solid blue and pink lines cover the observed wavelength range for MagE orders #9–14. The dashed lines are extrapolations to longer wavelengths. The star component is represented by a 4400 K blackbody spectrum. The blue line represents a power-law model obtained by fitting the observed relative flux of disk emission (filled blue squares) in the six orders, excluding the data point for order #13 (the second blue square from the left),, which is a clear outlier. The black dotted lines show the effective wavelengths of the *R*, *I*, *J*, *H*, *K* bands. Our estimate of the disk veiling factor in each band is also labeled.

tio and the value of the mass function given in §3.2, the masses of the black hole and secondary star are $M = 3.52 \pm 0.07(\sin^{-3} i)\ M_\odot$ and $M_2 = 0.28 \pm 0.03(\sin^{-3} i)\ M_\odot$, respectively.

4.2. *Disk Veiling*

The disk veiling factor $f_{\rm disk}$, i.e., the fraction of the total light that is non-stellar, is also determined by the optimal subtraction method. For each order, we first broaden the HD 170493 template spectrum using the values of $v \sin i$ determined in §4.1, and then optimally subtract it from the spectrum of NovaMus. The procedure gives the fraction of light due to the secondary star, $f_{\rm star}$, for the template spectrum that corresponds to the minimum value of χ^2. The disk veiling factor is then simply $f_{\rm disk} = 1 - f_{\rm star}$. As in determining $v \sin i$ we computed $f_{\rm disk}$ using for each order the averaged, rest-frame spectrum of NovaMus. The values we adopt for the disk veiling factor for the six orders are indicated in Fig. 6 by dotted lines and are listed in the last column of Table 3.

As a check on the robustness of our measured values of $f_{\rm disk}$, we repeated the optimal subtraction procedure for each spectrum individually, using only those spectra that produced a reliable measurement of radial velocity (see §3). A histogram of $f_{\rm disk}$ for each order is shown in Fig. 6; the dashed line in each panel represents the weighted mean value of the disk veiling factor. These alternative measurements of $f_{\rm disk}$, are consistent within $\sim 1\sigma$ (for all orders) with the values determined as described above using the phase-averaged spectra. We note that for five of the six orders $f_{\rm disk}$ is greater than 0.5, i.e., the disk is brighter than the secondary star.

Fig. 6 indicates that the disk veiling factor generally decreases with increasing wavelength, i.e., the disk veiling is less significant for redder wavebands. However, this does not necessarily mean that disk veiling can be ignored, even in the *J* and *K* bands, as claimed by Gelino et al. (2001) and others. We utilize a simplistic spectral energy distribution (SED) model and an extrapolation to illustrate this point (see Fig. 7). Our crude SED by no means represents an accurate model of the disk emission. For the stellar component, we assumed blackbody emission at 4400 K (red line in Fig. 7; see §3 and Fig. 2), and we then computed the relative disk flux in each order (filled blue squares) based on our measurements of $f_{\rm disk}$. We fitted these estimates of disk flux using a power-law model to represent the SED of the disk component and then extrapolated the power law into the near-infrared (dashed blue line).

At shorter wavelengths, the disk component does indeed decrease rapidly with increasing wavelength so that the stellar component becomes dominant as one approaches the *R*-band. However, at longer wavelengths the blackbody component begins to fall rapidly, and disk veiling reaches a minimum ($\approx 40\%$) at around 1 μm and then begins to increase. For our data and this crude model, we estimate that $f_{\rm disk}$ for the *I*, *J*, *H*, *K* bands is in the range of 40–60% (see the black dotted lines in Fig. 7), which is consistent with the estimates of Reynolds et al. (2008) for NovaMus of 40–50% in the near-infrared. We note that $f_{\rm disk}$ in the near-infrared could be lower than our estimate if the disk component of emission has a thermal spectrum that falls below the extrapolated power-law spectrum, which we assume. However, we conclude that it is not warranted to assume that the effects of veiling are negligible in the near-infrared.

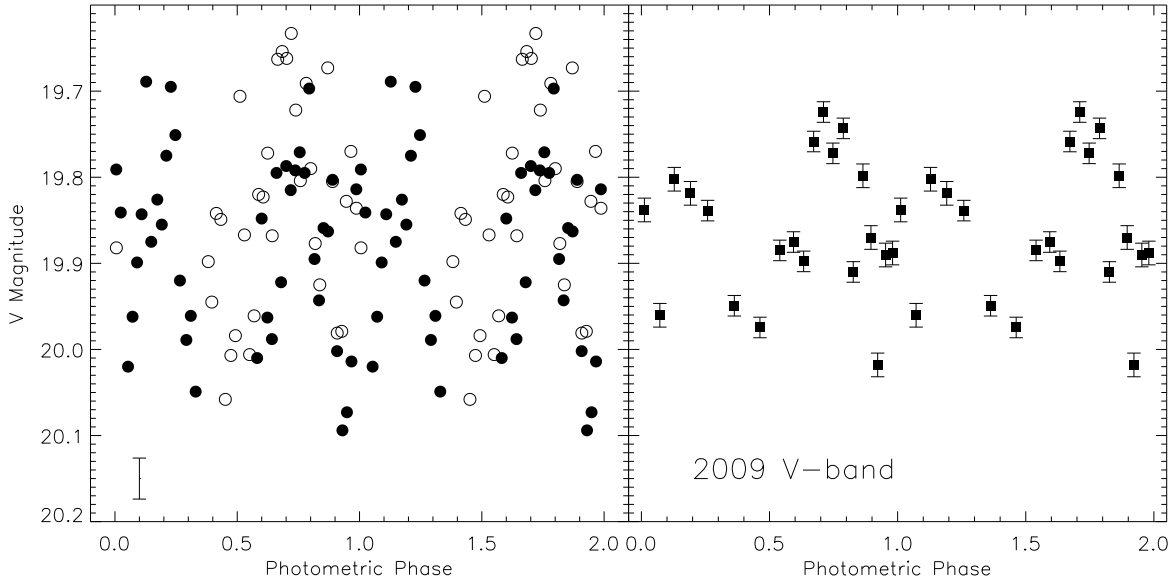

FIG. 8.— The original (left panel) and phase-binned (right panel) V-band light curves of NovaMus, acquired with the du Pont 2.5-m Telescope. In the left panel, the open (filled) circles are the photometry data points obtained during the first (second) night of observation. The error bar in the lower left corner represents the typical uncertainty. In the right panel, the light curve is binned into 20 phase bins, each of which has three or four individual data points.

5. LIGHT CURVE

Our calibrated and phase-folded V-band light curve, which was obtained in exposures that obtained simultaneously with the spectroscopic exposures (see §2.2), is shown in Fig. 8. Zero photometric phase, which is equivalent to 0.75 spectroscopic phase, corresponds to the inferior conjunction of the secondary. Two versions of the light curve are shown, unbinned and binned into 20 phase bins, each with 3–4 data points per bin.

During our observations, NovaMus was ~ 0.5 magnitude brighter on average in the V-band than it was in earlier photometric monitoring campaigns (e.g., during 1992–1995, as reported by Orosz et al. 1996). Our V-band light curve shows substantial aperiodic flickering (see §6.2). Nevertheless, the phase-binned light curve exhibits the characteristic signatures of ellipsoidal modulation, with two minima at phases ~ 0.0 and ~ 0.5 and two maxima at phases ~ 0.25 and ~ 0.75. The two maxima do not have equal amplitude as one would expect for an ideal ellipsoidal modulation, which could be caused by a hot spot in the accretion disk. Such unequal maxima have frequently been observed in the light curves of other black hole binaries in quiescence, e.g., A0620−00 (McClintock & Remillard 1986; Cantrell et al. 2010).

6. DISCUSSION

6.1. *Assessment of Systematic Uncertainties*

We identify sources of systematic error, and obtain estimates of their magnitude, first for the orbital parameters K_2 and T_0 and the systemic velocity γ, and then for the rotational velocity $v \sin i$.

6.1.1. *Orbital Parameters and Systemic Velocity*

We first consider the uncertainty associated with the choice of template spectrum. While we chose the spectrum of HD 107493 because it gave the maximum TDR value (§3.1), obviously this spectrum is not identical to that of the Roche-lobe-filling companion star. Focusing on the high-quality data for order #12, we repeated our analysis for six other template spectra with TDR values > 60 (see Fig. 2); the results are summarized in Table 4. The spread in the values of K_2 is < 0.8 km s^{-1}, which is significantly smaller than the statistical uncertainty. As our estimate of the systematic error in K_2 associated with the choice of the template, we take the standard deviation of the seven values of K_2, which is 0.3 km s^{-1}. In like manner, we obtain estimates of systematic error of 4.2 km s^{-1} for γ, and of 0.00013 day for T_0.

A second source of systematic uncertainty is the effect of the different widths of the photospheric lines for NovaMus which are rotationally broadened, and for the slowly-rotating template star, which are narrow. To assess this effect, we broadened the lines of our chosen template (HD 107493) to 85 km s^{-1} (§4.1) and repeated the radial velocity analysis. The change in K_2 is 0.5 km s^{-1} (Table 4), which we adopt as our estimate of systematic error; we obtain similar estimates of systematic error for γ and T_0 of 0.8 km s^{-1} and 0.00020 day, respectively.

For each of the three parameters in question, we obtain our final estimate of error, which is given in Table 2, by linearly adding the larger of the two systematic errors discussed above onto the statistical error obtained in §3.2 (given in Table 1).

6.1.2. *Rotational Velocity*

We identify two sources of systematic uncertainty for $v \sin i$, namely, the value adopted for the limb darkening coefficient and the choice of template spectrum. Again, using the data for order #12, we considered an uncertainty of ± 0.1 in our adopted value of 0.845 (Table 3) and find that this corresponds to an uncertainty of ≤ 1.5 km s^{-1} (see Table 5). We then

TABLE 4
RADIAL VELOCITY ANALYSIS RESULTS FOR DIFFERENT TEMPLATES (ORDER #12)

Templates (Order #12)	$B-V$	Template γ (km s^{-1})	TDR	K_2 (km s^{-1})	γ (km s^{-1})	$T_0-2454900$ (d)	No. of Object Spectra	χ^2/ν
HD 147776	0.95	7.4 ± 0.1	60.8	402.0 ± 2.7	17.1 ± 2.0	46.90339 ± 0.00044	72	0.83
HD 130992	1.02	-57.1 ± 0.1	64.1	401.9 ± 2.7	10.9 ± 2.0	46.90333 ± 0.00044	72	0.79
HD 31560	1.09	6.4 ± 0.1	74.3	401.6 ± 2.7	11.4 ± 2.0	46.90332 ± 0.00044	72	0.81
HD 170493	1.11	-55.1 ± 0.1	78.4	401.2 ± 2.6	9.7 ± 1.9	46.90327 ± 0.00044	72	0.87
HD 170493 (broadened)	1.11	-55.1 ± 0.1	76.7	401.7 ± 3.0	10.5 ± 2.2	46.90347 ± 0.00050	72	0.60
HD 131977	1.11	26.8 ± 0.1	65.9	401.6 ± 2.7	10.9 ± 2.0	46.90326 ± 0.00045	72	0.79
HD 156026	1.16	0.1 ± 0.1	61.6	401.9 ± 2.8	4.6 ± 2.0	46.90344 ± 0.00046	72	0.87
HD 120467	1.26	-37.8 ± 0.1	63.1	401.9 ± 2.8	5.5 ± 2.1	46.90365 ± 0.00047	72	0.79

TABLE 5
ROTATIONAL VELOCITY FOR DIFFERENT TEMPLATES
(ORDER #12)

Template	$B-V$	u (limb darkening)	$v\sin i$ (km s^{-1})
HD 170493	1.11	0.845	82.8 ± 3.5
HD 170493	1.11	0.745	81.7 ± 3.6
HD 170493	1.11	0.945	84.3 ± 3.7
HD 147776	0.95	0.823	82.9 ± 4.6
HD 130992	1.02	0.842	82.3 ± 4.5
HD 31560	1.09	0.845	82.4 ± 4.2
HD 131977	1.11	0.845	82.3 ± 4.0
HD 156026	1.16	0.835	83.8 ± 4.3
HD 120467	1.26	0.796	85.5 ± 5.2

NOTE. — The quoted uncertainties are at the 1σ level of confidence.

compared values of $v\sin i$ derived using once again the six template spectra with TDR values >60. For each template spectrum, we used the appropriate limb darkening coefficient (Claret et al. 2012) based on the $B-V$ color and corresponding effective temperature of the star. The standard deviation for the six values of $v\sin i$ is 1.2 km s^{-1}. Using these two estimates of systematic error as a guide, we allow for systematic error by simply doubling the statistical error bar obtained in §4.1 (1.3 km s^{-1}). Our final adopted value of $v\sin i$ given in Table 2, is therefore 85.0 ± 2.6 km s^{-1}

6.2. *Comparison to Previous Work*

We have obtained precise measurements of the mass function $f(M)$ and mass ratio q for NovaMus using multi-order echellette spectral data obtained with Magellan/MagE. Compared to the data analyzed in previous work (e.g., Orosz et al. 1996 and Casares et al. 1997), our spectra have higher spectral resolution (by a factor of $\sim$ 3–5) and provide more complete phase coverage. We also observed many more template stars (38), all of them during the same observing run, which has enabled us to choose a template spectrum that is an exceptionally close match to the spectrum of NovaMus. Analyzing data independently for several orders is also a feature of our work. All of these beneficial factors have contributed to quality of our work.

Our value for the radial velocity amplitude ($K_2=406.8\pm2.7$ km s^{-1}) is very close to that obtained by Orosz et al. (1996; $K_2=406\pm7$ km s^{-1}), while the uncertainty has been reduced significantly. Meanwhile, our K_2 value is barely consistent with that of Casares et al. (1997; $K_2=420.8\pm6.3$ km s^{-1}), differing by $\approx 2\sigma$. We have substantially increased the precision of the orbital period (by a factor of >30) by extending the baseline of observations from those made earlier (Remillard et al. 1992; Orosz et al. 1996) out to our observations in 2009.

Our mass ratio ($q=0.079\pm0.007$) agrees with the approximate value ($0.0476<q<0.0833$) found by Antokhina & Cherepashchuk (1993), which was obtained by modeling an I-band light curve. It is significantly smaller than the less reliable estimate of $q=0.133\pm0.019$ obtained by Orosz et al. (1996; see §1). Casares et al. (1997), who used the same direct method of measurement we used, likewise obtained a mass ratio greater than ours, $q=0.13\pm0.04$. (Their estimate of the rotational broadening is $v\sin i=106\pm13$ km s^{-1} compared to our value of $v\sin i=85.0\pm2.6$ km s^{-1}.) The relative virtues of our measurement is our better spectral resolution ($\approx$ 60 km s^{-1} at $\sim$ 5000 Å) and our ample selection of template spectra, which allowed us to closely match the spectrum of the donor star; Casares et al. had applied a single template spectrum of a K0V star.

An important feature of our work is the simultaneity of the spectroscopic and photometric observations, which allows one to accurately correct for the effects of disk veiling, despite the aperiodic variability of the non-stellar component of light. Unfortunately, during our observation NovaMus was in an "active" quiescent state (Cantrell et al. 2008), and the light curve is strongly affected by aperiodic flickering and does not provide a useful constraint on the inclination angle. Nevertheless, our simultaneous observations provide very secure measurements of the disk veiling factor at six wavelengths. In a subsequent paper, we will use these data in conjunction with light curves available in the literature, which were obtained in the "passive" quiescent state (Cantrell et al. 2008) to constrain the inclination angle and black hole mass.

6.3. *The Li λ6708 Feature*

The Li λ6708 absorption line was previously detected in the spectra of NovaMus (Martín et al. 1996). This feature also appears in the spectra of other similar black hole soft X-ray transients like A0620−00 (Marsh et al. 1994) and GS 2000+25 (Filippenko et al. 1995). This feature is potentially relevant in exploring the Li production mechanism around a black hole (Martín et al. 1994). Meanwhile, the variation of the line intensity with orbital phase may reveal effects of irradiation on the formation of the Li feature (Martín et al. 1996).

We find that the Li λ6708 line is marginally detected in the phase-averaged spectrum of NovaMus and also in the residual

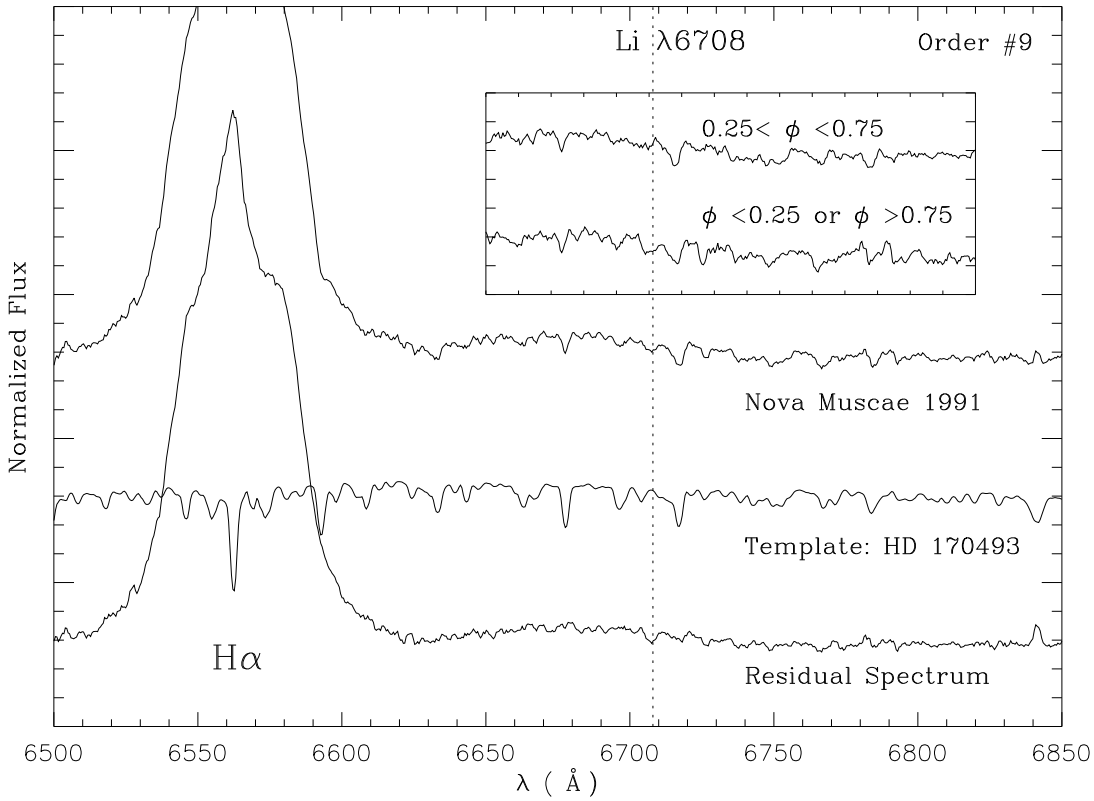

FIG. 9.— The averaged spectrum of NovaMus (top), the template spectrum of HD 170493 (middle), and the residual spectrum (bottom) after optimal subtraction, all for MagE order #9 and in the heliocentric frame. The location of Li λ6708 is indicated by the dotted line. This Li absorption feature is marginally detected ($\sim 3.5\sigma$). The inset plot shows the phase-resolved NovaMus spectra around Li λ6708. The Li feature is detected in the lower spectrum, in which the photometric phase ϕ is around zero ($\phi > 0.75$ or $\phi < 0.25$). There is no clear Li feature in the upper spectrum around photometric phase 0.5 ($0.25 < \phi < 0.75$). All the spectra are smoothed with a 5-pixel boxcar for the purpose of presentation.

spectrum after optimal subtraction (Fig. 9). We find an equivalent width of EW(Li)$= 210 \pm 60$ mÅ, after correcting for the disk veiling in order #9, for the NovaMus spectrum averaged over the full orbital phase. Following Martín et al. (1996), we investigated the variation of the EW(Li) with orbital phase (see the inset plot of Fig. 9). At zero photometric phase ($\phi > 0.75$ or $\phi < 0.25$), we obtained EW(Li)$= 550 \pm 90$ mÅ, which is slightly higher than the value in Martín et al. (1996; 420 ± 60 mÅ). The Li λ6708 feature is not detected at photometric phase 0.5 ($0.25 < \phi < 0.75$), which agrees with the findings in Martín et al. (1996). We note that our EW(Li) for NovaMus is slightly higher (within 1σ) than the value reported for A0620−00 of EW$= 160 \pm 30$ mÅ by Marsh et al. (1994).

We thank the anonymous referee for a careful reading of the manuscript and the helpful comments. We thank T. Marsh for developing and sharing the MOLLY spectral analysis software. J.E.M. acknowledges the support of NASA grant NNX11AD08G. D.S. acknowledges support from the Science and Technology Facilities Council, grant number ST/L000733/1. L.J.G. and L.C.H. acknowledge the support by the Chinese Academy of Sciences through grant No. XDB09000000 (Emergence of Cosmological Structures) from the Strategic Priority Research Program. L.J.G. acknowledges the support by National Natural Science Foundation of China (grant No. 11333005) and by National Astronomical Observatories of China (grant No. Y234031001). L.C.H acknowledge the support by the National Natural Science Foundation of China through grant No. 11473002.

Support for the design and construction of the Magellan Echellette Spectrograph was received from the Observatories of the Carnegie Institution of Washington, the School of Science of the Massachusetts Institute of Technology, and the National Science Foundation in the form of a collaborative Major Research Instrument grant to Carnegie and MIT (AST0215989).

Facility: Magellan:Clay (Magellan Echellette Spectrograph), du Pont

REFERENCES

Antokhina, E. A., & Cherepashchuk, A. M. 1993, Astronomy Letters, 19, 194
Cantrell, A. G., Bailyn, C. D., McClintock, J. E., & Orosz, J. A. 2008, ApJ, 673, L159
Cantrell, A. G., Bailyn, C. D., Orosz, J. A., et al. 2010, ApJ, 710, 1127
Casares, J., Martín, E. L., Charles, P. A., Molaro, P., & Rebolo, R. 1997, New A, 1, 299
Claret, A., Hauschildt, P. H., & Witte, S. 2012, A&A, 546, AA14
della Valle, M., Jarvis, B. J., & West, R. M. 1991, Nature, 353, 50
Ebisawa, K., Ogawa, M., Aoki, T., et al. 1994, PASJ, 46, 375
Esin, A. A., McClintock, J. E., & Narayan, R. 1997, ApJ, 489, 865
Filippenko, A. V., Matheson, T., & Barth, A. J. 1995, ApJ, 455, L139
Fragos, T., & McClintock, J. E. 2014, ApJ, submitted (arXiv:1408.2661)
Freeman, P. E., Kashyap, V., Rosner, R., & Lamb, D. Q. 2002, ApJS, 138, 185
Gelino, D. M., Harrison, T. E., & McNamara, B. J. 2001, AJ, 122, 971
Goldwurm, A., Ballet, J., Cordier, B., et al. 1992, ApJ, 389, L79
Hawking, S. 1971, Phys. Rev. Lett., 26, 1344

Israel, W. 1967, Phys. Rev., 164, 1776
Kaiser, C. R., & Hannikainen, D. C. 2002, MNRAS, 330, 225
Kalogera, V., & Baym, G. 1996, ApJ, 470, L61
Lund, N., & Brandt, S. 1991, IAU Circ., No. 5161
Makino, F., & The Ginga Team 1991, IAU Circ., No. 5161
Marsh, T. R., Robinson, E. L., & Wood, J. H. 1994, MNRAS, 266, 137
Marshall, J. L., Burles, S., Thompson, I. B., et al. 2008, Proc. SPIE, 7014,
Martín, E. L., Casares, J., Molaro, P., Rebolo, R., & Charles, P. 1996, New A, 1, 197
Martín, E. L., Rebolo, R., Casares, J., & Charles, P. A. 1994, ApJ, 435, 791
McClintock, J. E., Narayan, R., & Steiner, J. F. 2014, Space Sci. Rev., 183, 295
McClintock, J. E., & Remillard, R. A. 1986, ApJ, 308, 110
Moore, C. E., 1972, A Multiplet Table of Astrophysical Interest, National Bureau of Standards, Washington, p.66
Morningstar, W. R., Miller, J. M., Reis, R. C., & Ebisawa, K. 2014, ApJ, 784, L18
Narayan, R., & Yi, I. 1994, ApJ, 428, L13
Nidever, D. L., Marcy, G. W., Butler, R. P., Fischer, D. A., & Vogt, S. S. 2002, ApJS, 141, 503
Orosz, J. A., Bailyn, C. D., McClintock, J. E., & Remillard, R. A. 1996, ApJ, 468, 380
Orosz, J. A., Bailyn, C. D., Remillard, R. A., McClintock, J. E., & Foltz, C. B. 1994, ApJ, 436, 848
Ratti, E. M., van Grunsven, T. F. J., Jonker, P. G., et al. 2013, MNRAS, 428, 3543
Ratti, E. M., Steeghs, D. T. H., Jonker, P. G., et al. 2012, MNRAS, 420, 75
Remillard, R. A., & McClintock, J. E. 2006, ARA&A, 44, 49
Remillard, R. A., McClintock, J. E., & Bailyn, C. D. 1992, ApJ, 399, L145
Reynolds, M. T., Callanan, P. J., & Filippenko, A. V. 2007, MNRAS, 374, 657
Reynolds, M. T., Callanan, P. J., Robinson, E. L., & Froning, C. S. 2008, MNRAS, 387, 788
Shakura, N. I., & Sunyaev, R. A. 1973, A&A, 24, 337
Steeghs, D., & Jonker, P. G. 2007, ApJ, 669, L85
Sunyaev, R., Churazov, E., Gilfanov, M., et al. 1992, ApJ, 389, L75
Tonry, J., & Davis, M. 1979, AJ, 84, 1511
Wade, R. A., & Horne, K. 1988, ApJ, 324, 411